Influence of Aft Deck on the Flow Characteristics of a Serpentine Shock Vector Control Nozzle

LIANG Shuang, SHI Jingwei, WANG Zhanxue*

School of Power and Energy, Northwestern Polytechnical University, Xi'an 710000, P. R. China

(Received 28 October 2022; revised 3 February 2023; accepted 12 February 2023)

Abstract: A convergent-divergent serpentine shock vector controlling nozzle can significantly reduce the infrared and electromagnetic radiation intensity of the engine tail, and realize the thrust vector control in the pitch direction of supersonic aircraft, which greatly enhances the stealth and maneuverability of the aircraft. As the nozzle with a rectangular outlet needs to be integrated with the rear fuselage, one side wall is usually extended as an aft deck, so that the deflection rule of the tail jet is different from that under the symmetrical nozzle outlet. In this paper, numerical simulation is used to compare the flow characteristics of serpentine shock vector controlling nozzle with and without an aft deck, and then the influences of the aft deck length and angle on the performance of serpentine shock vector controlling nozzle with an aft deck are studied respectively. The results show that under certain working conditions, the oblique shock wave induced by secondary flow injection from the upper wall will be reflected from the aft deck, which is not conducive to the generation of downward thrust vector angle. When there is no open separation of the aft deck surface, the outflow from the lower wall will flow along the aft deck surface, so the increase of the length or angle of the aft deck will deflect the jet velocity axis downward.

Key words: aft deck; serpentine nozzle; thrust vectoring nozzle; shock vector controlling; flow characteristic

CLC number: TN925 **Document code:** A **Article ID:** 1005-1120(2023)01-0013-12

0 Introduction

The blended-wing body has been proved to have the advantages of large lift-drag ratio, low radar scattering area, high space utilization rate, and has played a huge advantage in the military field[1-2]. Super stealth, high maneuverability and wide speed range are crucial to the survival and combat capability of blended-wing body fighters[3-4]. These advanced aircraft performances are closely related to the design of the engine exhaust system, which needs to be designed with low detectability, thrust vector and high thrust-weight ratio.

The infrared and electromagnetic signals of the exhaust system can be the significantly reduced by the serpentine stealth nozzle[5]. The nozzle buried deeply within the body in order to reduce the exposure area of hot wall, the curved flow channel can shield the high-temperature parts of the engine (such as the plate after the turbine, the tail cone, afterburner, etc.) and reflect to weaken incoming electromagnetic waves for many times, and the flat outlet can reduce the high temperature core region of the jet by strengthening the mixing of the jet and the surrounding cold air[6]. The convergent and divergent channel can obtain supersonic jet, greatly increase the engine thrust, and meet the requirements of supersonic cruise/penetration[7].

The shock vector control (SVC) method is a suitable thrust vector technology for the fixed geometry nozzle with a high thrust-to-weight ratio[8]. The principle of this technology is to inject high pressure secondary flow into the supersonic mainstream in the expansion section of the nozzle, and induce an

*Corresponding author, E-mail address: shijw@nwpu.edu.cn.

How to cite this article: LIANG Shuang, SHI Jingwei, WANG Zhanxue. Influence of aft deck on the flow characteristics of a serpentine shock vector control nozzle[J]. Transactions of Nanjing University of Aeronautics and Astronautics, 2023, 40(1): 13-24.

http://dx.doi.org/10.16356/j.1005-1120.2023.01.002

oblique shock wave at the upstream of the secondary flow nozzle. After the mainstream passes through the shock wave, the streamline deflects downward to generate a thrust vector. Compared with the mechanical vector nozzle, this pneumatic vector nozzle does not need moving parts and actuating parts, and only by the injection of secondary flow can realize the mainstream micro vector regulation, meeting the conventional maneuver operation[9]. In addition, the shock vector control technology has a good control effect on supersonic airflows, and can work in a wider range of pressure ratio conditions. So it is more suitable for serpentine convergent-divergent nozzle with large thrust-weight ratio.

In order to avoid destroying the integrity of the wing-body fusion aircraft and resulting in the degradation of aircraft aerodynamic and stealth performance, the nozzle should be well integrated with the aircraft aft-body in the design[10-11]. The curvature of the upper surface of the fuselage is large, but the curvature of the lower surface is small. Therefore, the fusion position of the nozzle and the lower surface of the fuselage is later than that of the upper fuselage, so the lower wall of the nozzle continues to extend, forming an asymmetric nozzle outlet configuration with an aft deck.

For the general two-dimensional (2D) nozzle, the flow passage is symmetric, and the secondary flow injection on the upper wall and that on the lower wall will produce symmetric deflection effects. In this case, only one side of the injection is selected for the study on the deflection law of the jet flow. However, aft deck will significantly impact jet flow and wave structure of the serpentine SVC nozzle with aft-deck studied in this paper[12-13].

In order to study the effects of the aft deck, Section 1 compares the flow field characteristics of the nozzle with and without the aft deck. In Section 2, the influence of the length of the aft deck on the performance of the serpentine SVC nozzle with aft deck is studied. In Section 3, the effect of aft deck angle on the performance of the serpentine SVC nozzle with aft deck is studied.

1 Geometric Model and Definition of Performance Parameters

1.1 Geometric model

Fig.1 displays a 3D schematic diagram of the serpentine SVC nozzle with an aft deck. The nozzle consists of a serpentine section, an expansion section, and an aft deck. The secondary flow nozzle is located near the nozzle outlet, and the secondary flow is perpendicular to the X-direction at the expansion section.

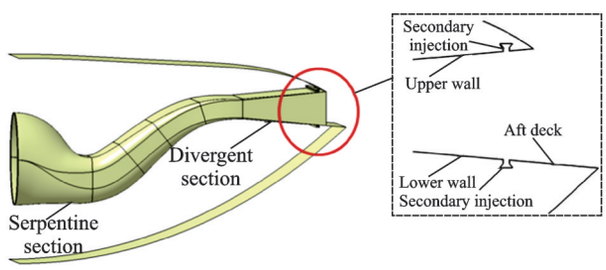

Fig.1 3D serpentine SVC nozzle with an aft deck

A 2D geometric model of the serpentine SVC nozzle with aft deck is established for numerical simulation, as shown in the Fig.2. The serpentine nozzle part is designed based on the Sun Xiaolin's design method[12]. The S-shaped center line is designed according to the Lee curve method. Parameter definitions of the 2D serpentine SVC nozzle with an aft deck are listed in Table 1.

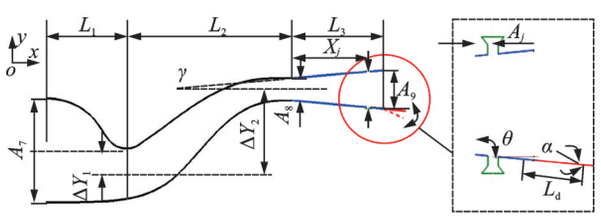

Fig.2 Parameter definitions of the serpentine SVC nozzle with aft deck

Table 1 Values of geometric parameters of serpentine SVC nozzle

Fixed parameter										Variable parameter	
A_7/A_8	A_9/A_8	L_1/A_8	L_2/A_8	L_3/A_8	$\Delta Y_1/A_8$	$\Delta Y_2/A_8$	A_j/A_8	X_j/L_3	γ/(°)	L_d/A_8	α/(°)
4.70	1.745	3.69	7.39	4.18	1.05	3.85	0.1	0.9	5	0.5—2.5	0—20

1.2 Parameter definition of the serpentine SVC nozzle with an aft deck

The thrust coefficient is an important parameter to measure the aerodynamic performance of the nozzle. For the thrust vectoring nozzle, the vectoring performance is generally measured by thrust vectoring angle and thrust vectoring efficiency. When calculating the performance parameters of the nozzle, the corresponding calculation is usually conducted based on the parameters of the nozzle outlet section. However, in this paper, the cut-off positions of the upper and the lower walls of the nozzle of the serpentine SVC nozzle with an aft deck are different, and the outlet section is difficult to define. Therefore, the cut-off position of the nozzle upper wall is defined as the nozzle outlet. However, the airflow parameters after the nozzle exit will continue to change along the aft deck, and the flow on the aft deck surface will continue to exert force on the nozzle. Therefore, the influence of the aft deck must be considered when calculating the performance parameters of the nozzle. The definition and calculation methods of three key performance parameters of the serpentine SVC nozzle with an aft deck that are concerned next.

1.2.1 Thrust vector angle

Thrust vector angle (δ_{p}) is one of the most critical performance parameters of the shock vector controlling nozzle. It is defined as the inverse tangent value of the ratio of the lateral component to the axial component of the nozzle thrust. Generally, the nozzle thrust can be calculated by the sum of the momentum thrust and the pressure difference thrust at the nozzle outlet. Since that the air flow will still exert force on the wall when it passes through the aft deck, the friction and pressure difference thrust on the aft deck surface should also be taken into account when calculating the thrust force of the nozzle.

The axial thrust force at nozzle outlet is defined as

$$F_{x,\mathrm{eff}}=F_{\mathrm{m}x}+F_{\mathrm{p}}+D_{\mathrm{p},x}-D_{\mathrm{f},x}=\sum_{i=1}^{n}\left(\rho V_{x,i}\cdot A_i\cdot V_{x,i}\right)+\sum_{i=1}^{n}\left(p_i-p_0\right)A_i+\cos\alpha\sum_{\text{aft deck}}\left(p-p_0\right)A_i+\sum_{\text{aft deck}}\tau_x A_i \tag{1}$$

where $F_{\mathrm{m}x}$, F_{p} are the axial momentum force and pressure difference thrust at the nozzle outlet; $D_{\mathrm{p},x}$ is the axial component of pressure difference thrust on the aft deck; $D_{\mathrm{f},x}$ the axial component of friction force on the aft deck; α the dip angle between the aft deck and the nozzle axis, and τ_x the axial component of the wall friction force.

The nozzle lateral thrust is defined as

$$F_{y,\mathrm{eff}}=F_{\mathrm{m}y}+D_{\mathrm{p},y}+D_{\mathrm{f},y}=\sum_{i=1}^{n}\left(\rho V_{x,i}\cdot A_i\cdot V_{y,i}\right)+\sin\alpha\sum_{\text{aftdeck}}\left(p-p_0\right)A_i+\sum_{\text{aftdeck}}\tau_y A_i \tag{2}$$

where $F_{\mathrm{m}y}$ is the lateral momentum force at the nozzle outlet; $D_{\mathrm{p},y}$ the lateral component of the pressure difference thrust on the aft deck; and $D_{\mathrm{f},y}$ the lateral component of the friction force on the aft deck.

Therefore, the thrust vector angle after considering the force of the aft deck is defined as

$$\delta_{\mathrm{p}}=F_{x,\mathrm{eff}}/F_{y,\mathrm{eff}} \tag{3}$$

1.2.2 Thrust coefficient

The thrust coefficient (C_{fg}) of the serpentine SVC nozzle with an aft deck is defined as the ratio of axial thrust to ideal thrust after considering the effect of pressure difference and friction on the aft deck.

The ideal thrust of the nozzle with the secondary flow injection is the sum of the ideal thrust $F_{i,\mathrm{noz}}$ of the nozzle and the ideal thrust $F_{i,\mathrm{sec}}$ of the secondary flow. $F_{i,\mathrm{noz}}$ and $F_{i,\mathrm{sec}}$ can be determined by one-dimensional isentropic flow equation

$$F_{i,\mathrm{noz}}=W_{\mathrm{noz}}\sqrt{\frac{2kR}{k-1}}\sqrt{T^*_{\mathrm{noz}}\left[1-\left(\frac{p_0}{p^*_{\mathrm{p}}}\right)^{\frac{k-1}{k}}\right]} \tag{4}$$

$$F_{i,\mathrm{sec}}=W_{\mathrm{sec}}\sqrt{\frac{2kR}{k-1}}\sqrt{T^*_{\mathrm{sec}}\left[1-\left(\frac{p_0}{p^*_{\mathrm{sec}}}\right)^{\frac{k-1}{k}}\right]} \tag{5}$$

where the subscript sec represents the secondary flow parameters; and noz the nozzle mainstream parameters.

The thrust coefficient is defined as

$$C_{\mathrm{fg}}=F_{x,\mathrm{eff}}/\left(F_{i,\mathrm{noz}}+F_{i,\mathrm{sec}}\right) \tag{6}$$

1.2.3 Thrust vector efficiency

Thrust vector efficiency (E_{V}) is defined as the

ability of a unit percentage of secondary flow to achieve thrust vector angle ((°)/%), and can be expressed as

$$E_V = \delta_p / \omega \sqrt{\tau} \tag{7}$$

where $\omega \sqrt{\tau}$ is the ratio of secondary flow to flow, and is calculated as

$$\omega \sqrt{\tau} = 100 \times \frac{W_{sec} \sqrt{T_{sec}}}{W_{noz} \sqrt{T_{noz}}} = 100 \times \frac{p^*_{sec} A_{sec} q(\lambda)_{sec}}{p^*_{noz} A_{noz} q(\lambda)_{noz}} \tag{8}$$

The performance parameters of the nozzle are affected by some parameters. The aerodynamic and geometric parameters affecting the performance of the serpentine SVC nozzle with the aft deck are as follows:

Nozzle pressure ratio (NPR): Ratio of the total pressure at the nozzle inlet to the back pressure at nozzle outlet.

Secondary flow pressure ratio (SPR): Ratio of the total pressure at the inlet of the secondary flow to the total pressure at the inlet of the nozzle main flow.

Dimensionless aft deck length (L_d/A_8): Ratio of aft the deck length to the nozzle throat height.

After deck angle (α): The angle of rotation from the positive X axis clockwise to the position of the aft deck.

2 Numerical Simulation

The numerical simulations of this study is carried out by using Fluent of ANSYS 19.2. The equations solved are the two-dimensional, compressible, Reynolds averaged, Navier-Stokes equations, which are discretized in the finite volume form on each of the quadrangle control volumes. The implicit density-based algorithm is used to solve the equation. The second order upwind scheme is used in the spatial discretization, and second implicit scheme is adopted for the time.

In the solving course, the choosing of the turbulent model will directly affect the prediction of flow details. As typical flow phenomena such as shock wave and flow separation are better predicted by shear stress transport (SST) k-ω model than other turbulence models[14-15], it is chosen to study the flow field characteristics of the serpentine SVC nozzle.

2.1 Computational grid

ANSYS ICEM software is used for numerical simulation in this paper to mesh the 2D geometric model of the serpentine SVC nozzle with an aft deck, and the calculation domain was divided into two parts: Nozzle domain and far field. The length and height of the far field area are 10 times of the axial length of the nozzle divergent section and the nozzle outlet height, respectively, so as to ensure that the calculation domain can fully display the wave system in the aft deck and downstream jet, and to avoid the influence of the far field on the nozzle flow and jet flow. The calculation grid is shown in Fig.3. In order to meet the requirements of SST k-ω turbulence model for wall $y+$, the mesh density of the boundary layer is increased, and the mesh height of the first layer is set to 0.005 mm, so that the wall $y+$ is controlled near 1. Due to the complex wave and vortex structures in the secondary flow injection area, the nozzle outlet, and the vicinity of the aft deck, the mesh density of the above areas is locally increased to accurately capture the flow details.

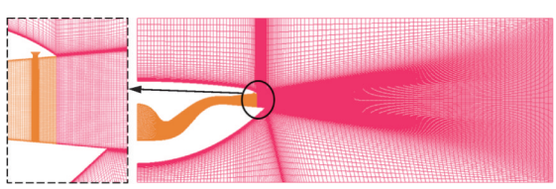

Fig.3 Meshing diagram of nozzle domain and far-field domain

2.2 Boundary conditions

The boundary division is shown in Fig.4. Reasonable setting of boundary conditions is the key to the convergence and accuracy of numerical simulations. The flow field and far field in the serpentine SVC nozzle with an aft deck studied in this paper include four boundary types: Pressure inlet boundary, pressure outlet boundary, far field boundary and solid wall boundary. Specific boundary conditions are set as follows:

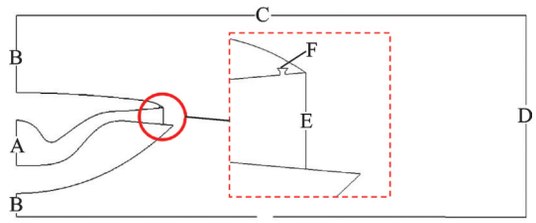

Fig.4 Schematic diagram for pulse generation and experimental results

A is the nozzle inlet and set as the boundary of the pressure inlet. The total pressure is given according to the requirement of the NPR of the nozzle. The total temperature is 300 K, and the airflow direction is perpendicular to the inlet surface.

B is the inlet of the far field and set as the pressure inlet boundary. The total pressure is 101.502 kPa, and the static pressure is 101.325 Pa. The total temperature is 300 K, and the incoming flow $Ma_\infty =$ 0.05, and the airflow direction is perpendicular to the inlet surface.

C is the lateral boundary of the far field and set as the far field boundary. The total temperature is 300 K, to flow $Ma_\infty =$ 0.05, and the incoming flow Ma_∞=0.05.

D is the outlet of the far field and set as the pressure outlet boundary. The total temperature is 300 K, and static pressure is 101.325 Pa.

E is the outlet of the nozzle and set as the inner face of the computational domain(interior).

F is the inlet of the secondary nozzle and set as the pressure inlet boundary. The total pressure is given according to the demand of the secondary flow pressure ratio of the nozzle, the total temperature is 300 K, and the airflow direction is perpendicular to the inlet surface.

The other edges in the computational domain are solid walls, and the boundary conditions are set as adiabatic no-slip boundaries.

2.3 Numerical simulation verification

At present, researchers have carried out many studies on the shock vector control technology. Some of the model test schemes are complete, reasonable, accurate, and provide many flow details, which can be used to verify the feasibility of the numerical simulation method in this paper. In this paper, the experimental results of Jet Exit Test Facility (JETF) conducted by NASA Langley Research Center are selected as the verification data[16]. The experimental model of the two-dimensional convergent-divergent nozzle is shown in Fig.5. The designed nozzle pressure ratio is 8.78, throat area is 0.401 062 4 m^2, and the breadth is 1.216 152 m. The profile parameters of the inner flow passage are shown in Fig. 6. The axial position of the throat is 0.729 691 2 m, the secondary flow is sprayed at 1.249 68 m, and the width of the secondary flow nozzle exit is 0.024 384 m.

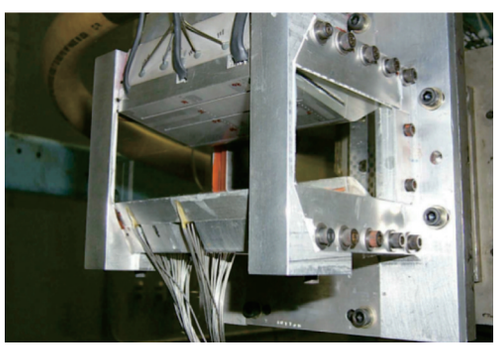

Fig.5 Test nozzle

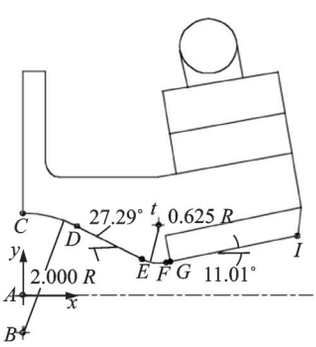

Point	Coordinate/m	
	X	Y
A	0.000 000 0	0.000 000 0
B	0.002 743 2	0.187 147 2
C	0.000 000 0	0.422 452 8
D	0.279 501 6	0.354 482 4
E	0.605 942 4	0.186 232 8
F	0.729 691 2	0.168 554 4
G	0.740 664 0	0.170 383 2
H	0.693 420 0	0.355 396 8
I	1.386 840 0	0.296 265 6

Fig.6 Nozzle flap contour

According to the geometric parameters of the symmetry plane of the 2D convergent-divergent nozzle, a 2D nozzle model is generated by using the geometric modeling software Catia, as shown in Fig.7.

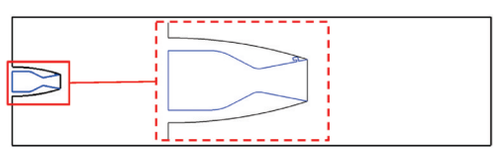

Fig.7 Numerical simulation model of binary convergent-divergent nozzle

By comparing the numerical simulation results of the pressure distribution curve on the upper wall of the nozzle with the experimental data, as shown in Fig.8, it can be seen that the wall pressure distribution predicted by the numerical simulation method adopted in this paper is in good agreement with the wall pressure distribution measured by the test. Through the superposition comparison of flow field results and experimental schlieren, as shown in Fig.9, it can be seen that the numerical simulation method adopted in this paper can well predict the position of each shock wave in the nozzle, and the prediction of induced shock wave, outlet shock wave and shock wave intersection is consistent with the test results.

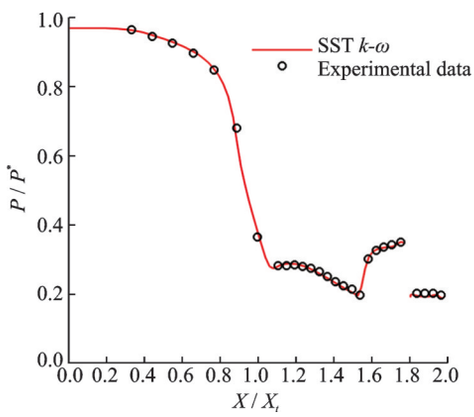

Fig.8 Comparison of the pressure distribution of the upper wall by numerical simulation with experimental data

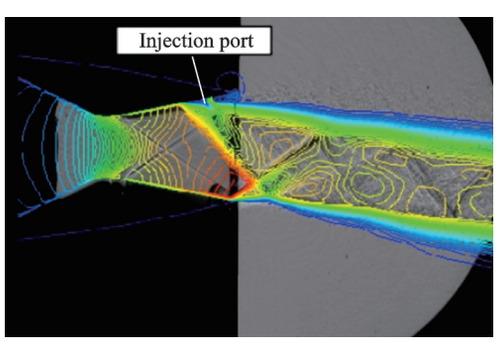

Fig.9 Comparison of the flow field predicted by numerical simulation with experimental Schlieren observation

Therefore, the numerical simulation method adopted in this paper has high reliability for the prediction of shock vector nozzle, and is suitable to simulate the serpentine SVC nozzle with aft deck in this paper.

3 Results and Discussion

3.1 Comparison of flow characteristics of serpentine shock vector controlling nozzle with and without an aft deck

For the serpentine SVC nozzle with an aft deck in this paper, the presence of the aft deck will significantly affect the wave structure in the nozzle and the wake flow, resulting in a significantly different flow deflection law from that of the serpentine SVC nozzle without an aft deck. Therefore, this section compares the flow fields of nozzles and wake flow with and without an aft deck.

For the general 2D nozzle, the flow passage is symmetric, and the secondary flow injection on the upper wall and the secondary flow injection on the lower wall will produce symmetric deflection effects. However, the aft deck results in different wave structure and jet deflection when injecting the secondary flows from the upper wall and from the lower wall. In this case, only the upper side of the injection is selected for the study on the deflection law of the jet flow.

Fig.10 compares the *Ma* contours of nozzles with and without an aft deck in the case of secondary flow injection on the upper wall with NPR=8 and SPR=0.4. When there is no aft deck, the separating shock wave emitting from the upper wall intersect with the free boundary below, and the jet is deflected downward by the shock wave. When there is an aft deck, the over-length of the aft deck will cause the oblique shock wave from the upper wall to hit the aft deck and reflect a diagonal shock wave from the lower wall. The oblique shock wave from the upper wall makes the jet direction deflect downward, while the reflected shock wave on the lower wall makes the jet direction deflect upward, which weakens the downward thrust vector effect produced by the secondary flow injection on the upper wall.

3.2 Influence of aft deck length on flow characteristics of serpentine shock vector controlling nozzle

When the aft deck angle is kept at 5°(the aft

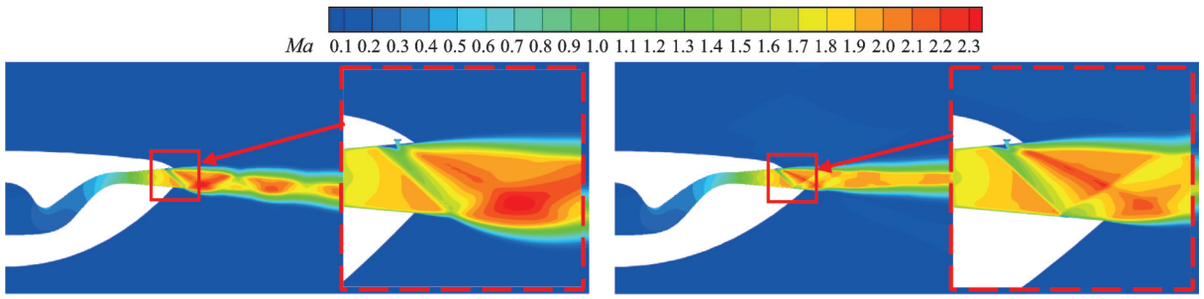

(a) *Ma* contour of the serpentine SVC nozzle without an aft deck (b) *Ma* contour of the serpentine SVC nozzle with an aft deck

Fig.10 Comparison of *Ma* contours of nozzles with and without aft deck

deck extends along the lower wall), and the dimensionless aft deck length is changed, the flow inside the nozzle and the deflection of the tail jet are shown in Fig.11. It can be seen that when the secondary flow is sprayed from the upper wall surface, the velocity axis of the tail jet gradually rotates upward with the increase of the length of the aft deck. The negative velocity vector angle of the wake gradually decreases to 0, and the thrust vector effect of the secondary flow injection on the upper wall is weakened by the increase of the length of the aft deck.

Therefore, the increase of the length of the aft deck reduces the control effect of the secondary flow on the deflection of the main stream.

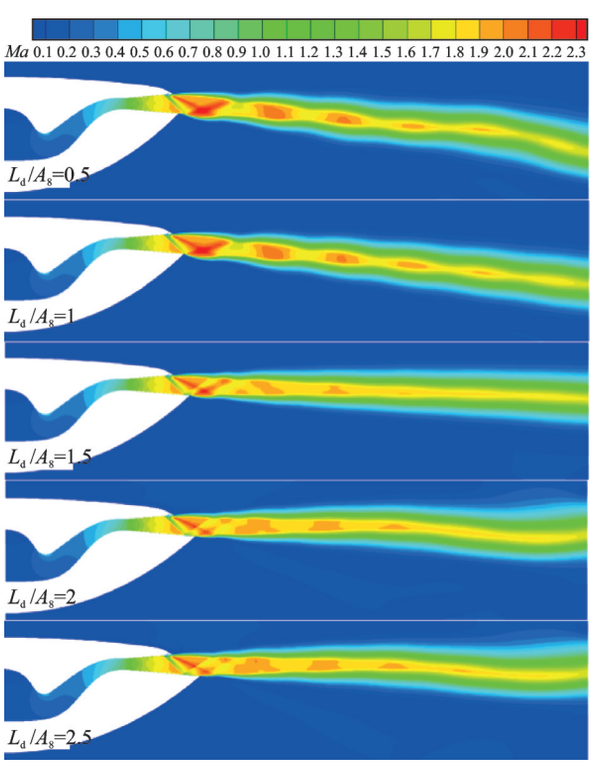

Fig.11 *Ma* contours of the serpentine SVC nozzle and tail jet under different aft deck lengths

With the increase of the length of the aft deck, the evolution of the flow field in the nozzle and the tail jet during the secondary flow injection on the upper wall of the nozzle is shown in Fig.12. With the increase of the length of the aft deck, the separation shock wave on the upper wall changes from the free shock wave to the restricted one, and the jet streamline at the outlet of the upper wall does not change obviously. The wave structure on the aft deck changes significantly, and the jet streamline at the tail edge of the aft deck gradually deflects upward with the increase of the length of the aft deck.

As can be seen from Fig.12, with the increase of the length of the aft deck, the wave system and vortex system structure on the upper wall remain unchanged. There is a wedge separation zone in front of the secondary flow nozzle and a closed separation zone behind the nozzle. A separation shock wave is emitted at the starting position of the wedge separation zone. A cluster of weak expansion waves is emitted at the position where the second flow reattaches to the upper wall. And a shock wave is emitted at the exit position of the upper wall. The flow near the upper wall of the nozzle and the outlet of the upper wall do not change with the increase of deck length. The entire lower wall of the nozzle, excluding the aft decks, is located before the intersection point between the separation shock wave and the lower boundary, so the flow state near the lower wall remains unchanged.

However, the wave system on the aft deck changes significantly with the increase of the length of the aft deck. When L_d/A_8=0.5, the separation shock wave emitted from the upper wall is an unre-

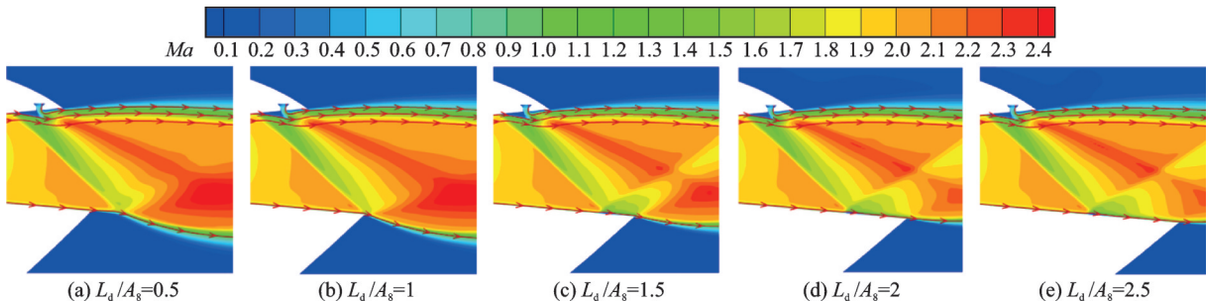

Fig.12 *Ma* contours and streamline diagrams near nozzle outlet under different aft deck lengths

stricted free shock wave, which intersects with the free boundary below and reflects a cluster of expansion waves. With the increase of the length of the aft deck, the separation shock wave begins to intersect with the aft deck when $L_d/A_8=1$, and reflects a weak oblique shock wave at the trailing edge of the aft deck. When $L_d/A_8=1.5$, $L_d/A_8=2$, $L_d/A_8=2.5$, the separation shock hit the aft deck and reflects a distinct oblique shock. With the increase of the length of the aft deck, the downward deviation angle of the jet streamline at the aft deck outlet gradually decreases. When $L_d/A_8=2.5$, the aft deck outlet jet is almost parallel to the X-axis direction.

The performance parameters of the nozzles at different aft deck lengths are further calculated, and the change law of the thrust vector angle varies with the aft deck length as shown in Fig.13(a). The change law of the thrust vector efficiency varies with the aft deck length, as shown in Fig.13(b), and the change law of thrust coefficient varies with the aft deck length, as shown in Fig.13(c).

As can be seen in Fig.13(a), when the length of the dimensionless aft deck increases from 0.5 to 1, the thrust vector angle increases to a peak value of about 4.3°. Then, with the increase of the aft deck length, the thrust vector angle decreases and remains at about 0° when $L_d/A_8=2$ and $L_d/A_8=2.5$. As shown in Fig.13(b), the thrust vector efficiency increases to a peak value of 1.26(°)/% and then decreases to 0 with the increase of the aft deck length, and becomes positive 0.01 (°)/% when $L_d/A_8=2.5$. As shown in Fig.13(c), with the increase of the length of the aft deck, the thrust coefficient decreases to a value of 0.975 when $L_d/A_8=1$, and then increases to a peak value of 0.981, and decreases again when $L_d/A_8=2.5$.

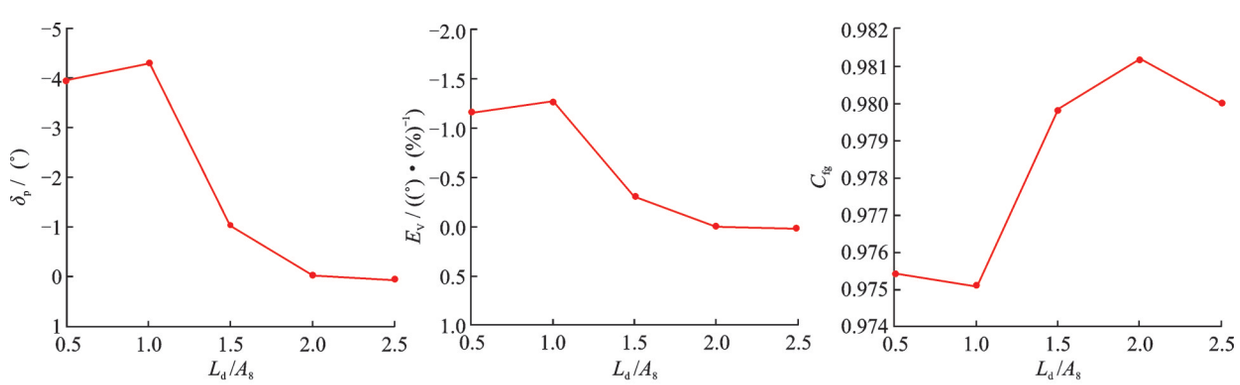

(a) Change law of thrust vector angle varies with the aft deck length (b) Change law of thrust vector efficiency varies with the aft deck length (c) Change law of thrust coefficient varies with the aft deck length

Fig.13 Change law of nozzle performance parameters varies with the aft deck length

In conclusion, the thrust vector angle is maximum when the upper wall separation shock hits the aft deck exit. When the separation shock wave intersects with the aft deck, the increase of the aft deck length is not conducive to the formation of the downward thrust vector angle of the nozzle.

3.3 Influence of aft deck angle on flow characteristics of serpentine shock vector controlling nozzle

The dimensionless length of the aft deck is kept unchanged as 1, and the angle of the aft deck is

changed. The flow inside the nozzle and the deflection of the tail jet are shown in Fig.14. It can be seen that when the secondary flow on the upper wall is injected, the velocity axis of the tail jet is always deflected downward at different angles of the aft deck (0°—20°), However, with the increase of the aft deck angle, when α is between 0° and 15°, the velocity axis of the tail jet gradually rotates downward, and when α is between 15° and 20°, the velocity axis slightly rotates upward.

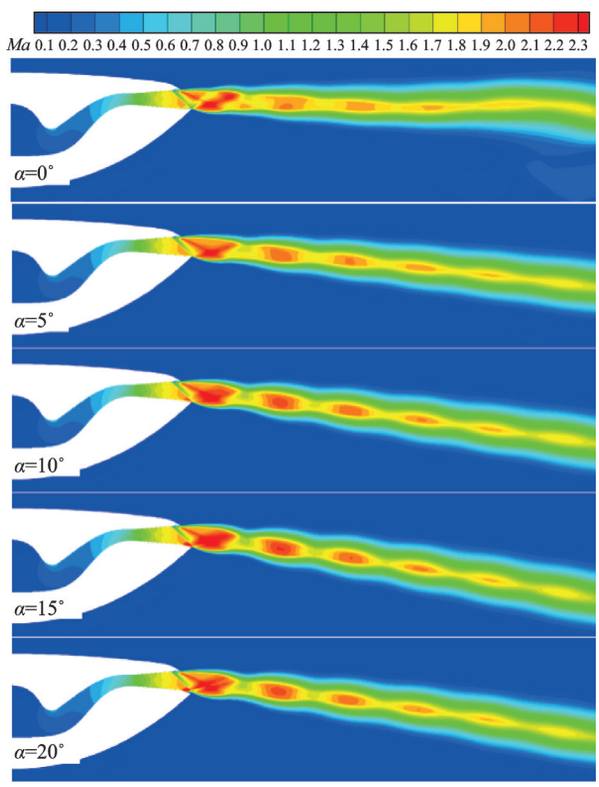

Fig.14 *Ma* contours of the serpentine SVC nozzle and tail jet under different aft deck angles

Therefore, the increase of the aft deck angle makes the jet velocity axis deflect downward before the flow separation occurs. But when the aft deck angle increases to a certain extent, the velocity axis will no longer deflect with the increase of the aft deck angle.

With the increase of the angle of the aft deck, the evolution of the flow field in the nozzle and the tail jet during the secondary flow injection on the upper wall of the nozzle is shown in Fig.15. As the aft deck angle is increased, the jet flow streamline at the upper wall outlet does not change obviously, and the upper wall separation shock changes from restricted shock to free shock. The wave structure on the aft deck changes significantly, and the jet streamline on the trailing edge of the aft deck gradually deflects downward with the increase of the angle of the aft deck. Flow separation occurs at $\alpha=20°$ on the aft deck. After the flow separation, the jet streamline is no longer deflected downward.

As can be seen from Fig.15, with the increase of the angle of the aft deck, the wave system and vortex system structures near the upper wall remain unchanged. There are a wedge separation zone in front of the secondary flow nozzle and a closed separation zone behind the nozzle. A separation shock wave is emitted from the initial position of the wedge separation region. A cluster of weak expansion waves is emitted from the secondary flow reattachment position. And a shock wave is emitted from the exit position of the upper wall.

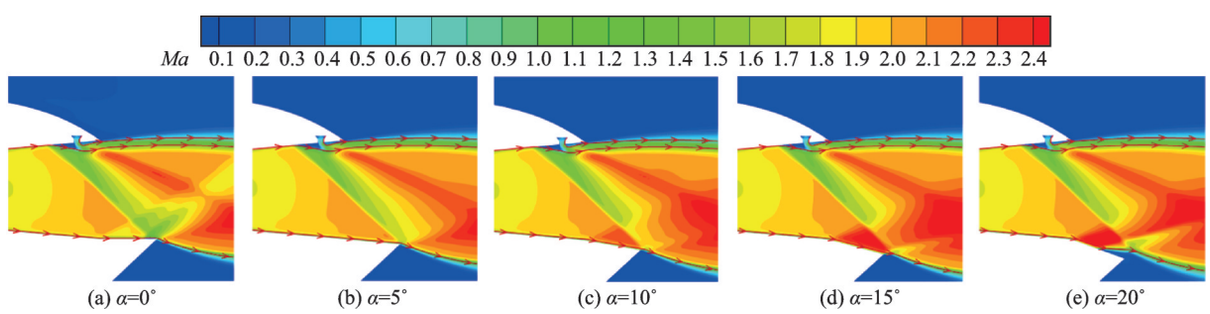

Fig.15 *Ma* contours and streamline diagrams near nozzle outlet under different aft deck angles

When $\alpha=10°$, $\alpha=15°$ and $\alpha=20°$, the air flow channel at the starting position of the aft deck is convex, and the air expands along the aft deck and sends out a cluster of expansion wave at the starting position of the aft deck. When $\alpha=10°$, the separation shock wave passes through the expansion wave

and hits the exit position of the aft deck, reflecting an oblique shock wave. When $\alpha=15^\circ$, the flow near the wall of the aft deck accelerates the expanding, resulting in the static pressure at the trailing edge of the quarterdeck being lower than the external atmospheric pressure. Therefore, an oblique shock wave is generated at the trailing edge of the aft deck. The separation shock wave on the upper wall first passes through the expansion wave formed by the convex flow passage, then passes through each other with the oblique shock wave on the trailing edge of the aft deck, and finally intersects with the free boundary and reflects a cluster of expansion wave. When $\alpha=20^\circ$, open separation occurs on the aft deck, and the separation point sends out an oblique shock wave. The separation shock wave on the upper wall first passes through the expansion wave formed by the convex flow channel, then passes through each other with the oblique shock wave issued by the separation point, and finally intersects with the free boundary, and reflects a cluster of expansion wave.

The performance parameters of the nozzles at different aft deck angles are further calculated, and the change law of the thrust vector angle varies with the aft deck angle, as shown in Fig.16(a). The change law of the thrust vector efficiency varies with the aft deck angle, as shown in Fig.16(b), and the change law of thrust coefficient varies with the aft deck angle, as shown in Fig.16(c).

As can be seen in Fig.16(a), with the increase of the aft deck angle, the negative thrust vector angle gradually increases, reaching a peak of 6.67° when $\alpha=15^\circ$. As shown in Fig.16(b), the thrust vector efficiency first increases and then decreases with the increase of the aft deck angle. When $\alpha=15^\circ$, the efficiency is the highest, which is 1.96(°)/%. As shown in Fig.16(c), the thrust coefficient decreases continuously with the increase of the aft deck angle, from 0.976 at $\alpha=0^\circ$ to 0.962 at $\alpha=20^\circ$.

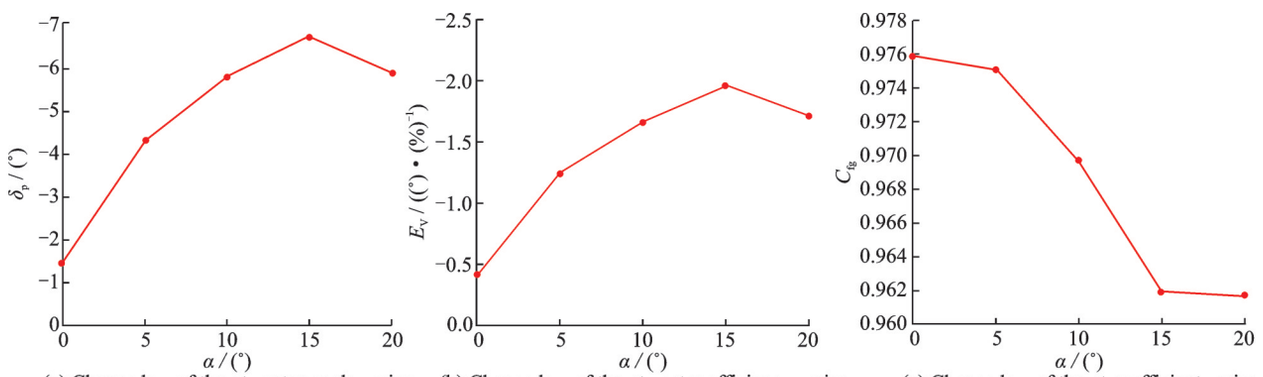

(a) Change law of thrust vector angle varies with the aft deck angle (b) Change law of thrust vector efficiency varies with the aft deck angle (c) Change law of thrust coefficient varies with the aft deck angle

Fig.16 Change law of nozzle performance parameters varies with the aft deck angle

In conclusion, when the dimensionless aft deck length is 1, the increase of the aft deck angle is conducive to the formation of the nozzle downward thrust vector angle before the flow separation occurs on the aft deck.

4 Conclusions

The flow characteristics a serpentine SVC nozzle with an aft deck are studied. The comparison of nozzle flow characteristics with and without an aft deck and the influence of the geometry parameters on the flow characteristics and performance of the nozzle are studied by the numerical simulation. The conclusions are drawn as follows:

(1) The difference in the flow characteristics of the serpentine SVC nozzle with and without an aft deck is obvious. The existence of the aft deck will make the separation shock wave caused by the secondary flow injection of the upper wall hit the afterdeck under certain working conditions and weaken the downward thrust vector effect produced by the secondary flow injection on the upper wall. The existence of the aft deck will make the air flow from the outlet of the lower wall flow along the aft deck

in certain working conditions, which can promote the formation of downward thrust vector angle.

(2) When separation shock wave intersects with the aft deck surface, the downward thrust vector angle decreases to 0 first and then turns to the upward thrust vector angle with the increase of the aft deck length. The thrust vector angle reaches the maximum when the separation shock exactly hits the aft deck exit.

(3) The thrust vector angle of the nozzle increases with the increase of the angle of the aft deck before the flow separation occurs.

(4) When NPR=8, SPR=0.4 and the aft deck angle $\alpha=5^\circ$, L_d/A_8 is in the range of 0.5—2.5, the maximum downward thrust vector angle generated by the secondary flow injection on the upper wall is about 4.3°, the maximum thrust vector efficiency is about 1.26°/%, and the maximum thrust coefficient is about 0.981.

(5) When NPR=8, SPR=0.4 and the dimensionless aft deck length $L_d/A_8=1$, α is in the range of 0.5°—2.5°, the maximum downward thrust vector angle generated by the secondary flow injection on the upper wall is about 6.67°, the maximum thrust vector efficiency is about 1.96(°)/%, and the maximum thrust coefficient is about 0.976.

References

[1] OKONKWO P, SMITH H. Review of evolving trends in blended wing body aircraft design[J]. Progress in Aerospace Sciences, 2016, 82: 1-23.

[2] JIMENEZ H, TETIK H, MAVRIS D. Assessment of operational compatibility for future advanced vehicle concepts[C]//Proceedings of the 50th AIAA Aerospace Sciences Meeting Including the New Horizons Forum and Aerospace Exposition. Nashville, USA: AIAA, 2012: 1-18.

[3] LIANG Chunhua, SUO Dejun, SUN Mingxia. A review on the key technologies of the sixth generation fighter engines in the US[J]. Aeroengine, 2016, 42(2): 93-97.(in Chinese)

[4] XU Dingguo, AI Junqiang, LEI Wutao, et al. Analysis on stealth requirement of next generation bomber in the future[J]. Advances in Aeronautical Science and Engineering, 2018(9): 1674-8190.(in Chinese)

[5] RAO G A, MAHULIKAR S P. Aircraft powerplant and plume infrared signature modelling and analysis[C]//Proceedings of the 43rd AIAA Aerospace Sciences Meeting and Exhibit. Reno, USA: AIAA, 2005: 1397-1407.

[6] WANG Zhanxue, YU Mengzhe, SHI Jingwei, et al. Study on flow mechanism and control method of ultra-compact S-shaped convergent-divergent nozzle[J]. Journal of Engineering Thermophysics, 2018, 39: 1718-1724.(in Chinese)

[7] CROWE D S, MARTIN C L. Effect of geometry on exit temperature from serpentine exhaust nozzles[C]//Proceedings of the 53rd AIAA Aerospace Sciences Meeting. Kissimmee, USA: AIAA, 2015.

[8] ZHANG Jiandong, WANG Zhanxue, LIU Zengwen, et al. Numerical simulation of two kinds of aerodynamic thrust vector techniques[J]. Acta Aerodynamica Sinica, 2012, 30: 206-209.(in Chinese)

[9] WING D J. Static investigation of two fluidic thrust-vectoring concepts on a two-dimensionl convergent-divergent nozzle: NASA Technical Memorandum-4574[R]. [S.l.]: NASA, 1994.

[10] JI H H Fundamental issues of aircraft/engine integration for low observability[R]. [S.l.] Aircraft/Engine Integration, 2018: 67-71.

[11] CARSON G T, LEE E E. Experimental and analytical investigation of axisymmetric supersonic cruise nozzle geometry at Mach numbers from 0.60 to 1.30: NASA TP 1953-C1[R].[S.l.]: NASA, 1981: 23-26.

[12] SUN Xiaolin, WANG Zhanxue, ZHOU Li, et al. Research on design method of serpentine stealth nozzle based on multi-parameter coupling[J]. Journal of Engineering Thermophysics, 2015, 36: 65-69.(in Chinese)

[13] BEHROUZI P, MCGUIRK J J. Underexpanded jet development from a rectangular nozzle with aft deck.[J]. AIAA Journal, 2015, 53: 1287-1298.

[14] SUN Xiaolin. Investigation on design method and performance estimation of low observable S-shaped nozzle[D]. Xi'an: Northwestern Polytechnical University, 2018.(in Chinese)

[15] SHI Jingwei. Investigation on flow mechanism and performance evaluation of fixed-geometric thrust vectoring nozzle[D]. Xi'an: Northwestern Polytechnical University, 2015.(in Chinese)

[16] KENRICK A, KAREN A. Experimental and computational investigation of multiple injection portsin a convergent-divergent nozzle for fluidic thrust vectoring [C]//Proceedings of the 21st Applied Aerodynamics Conference. Orlando, USA: AIAA, 2003: 1-14.

Acknowledgement The authors would like to acknowledge the following people for their assistance: WANG Wenjie, SUN Peng, QI Min, YE Yifan, HAO Wang, JIAO Liying, YANG Yuming, ZHANG Ziyu, LIN Zhifu, MENG Yubo, HUI Zhonghao, SHI Jie, all with the Jet Propulsion Research Laboratory, School of Power and Energy, Northwestern Polytechnical University.

Authors Ms. **LIANG Shuang** received her bachelor degree in flight vehicle propulsion engineering from the School of Power and Energy, Northwestern Polytechnical University, Xi'an, China, in 2016, and continued to study as a graduate student in the same school. Her research has focused on thrust vectoring nozzles, including mechanical thrust vectoring nozzles and pneumatic thrust vectoring nozzles.

Dr. **SHI Jingwei** received his bachelor degree from Nanjing University of Aeronautics and Astronautics, Nanjing, China, in 2009, and his M.S. and Ph.D. degrees from Northwestern Polytechnical University in 2012 and 2015, respectively. From July 2020, he works as an associate research fellow in the Jet Propulsion Research Laboratory, School of Power and Energy, Northwestern Polytechnical University. His main research interests include new exhaust system design technology, flow control technique, and modern flow field display and measurement technology.

Author contributions Ms. **LIANG Shuang** designed the study, complied the models, conducted the analysis, interpreted the results, and wrote the manuscript. Dr. **SHI Jingwei** guided the research, designed the article structure. Prof. **WANG Zhanxue** contributed to the discussion and background of the study. All authors commented on the manuscript draft and approved the submission.

Competing interests The authors declare no competing interest.

(Production Editor: ZHANG Bei)

后甲板对S弯激波矢量喷管流动特性的影响

梁 爽，史经纬，王占学

(西北工业大学动力与能源学院，西安 710000，中国)

摘要：收-扩型S弯激波矢量控制喷管不仅可以显著降低发动机尾部的红外和电磁辐射强度，还可以实现超声速飞机俯仰方向的推力矢量控制，极大地增强了飞机的隐身性和机动性。由于矩形出口需要与后机身融合，通常将下壁面延长作为后甲板，此时喷流的偏转规律与对称出口喷流的偏转规律不同。本文采用数值模拟的方法，比较了有后甲板和无后甲板S弯激波矢量控制喷管的流动特性，分别研究了有后甲板S弯激波矢量控制喷管的长度和角度对其性能的影响。结果表明：在某些工况下，上壁面二次流注入所诱导产生的斜激波会被后甲板反射，不利于向下推力矢量角的产生；当后甲板表面没有发生开式分离时，下壁面出口喷流会沿后甲板表面附壁流动，因此后甲板长度或角度的增加会使喷流速度轴线向下偏转。

关键词：后甲板；S弯喷管；推力矢量喷管；激波矢量控制；流动特性